Thermochimica Acta 475 (2008) 44–52

Contents lists available at ScienceDirect

Thermochimica Acta

journal homepage: www.elsevier.com/locate/tca

The oxidation mechanisms of $Cu_{54}Ni_{45}Mn_1$ (Constantan) tapes: Kinetic analysis

T.K. Jondo[a,b], Ph. Galez[b], J.-L. Jorda[b,*], J. Le Roy[b], J.C. Marty[b], J.L. Soubeyroux[c]

[a] Faculté des Sciences, Université de Lomé, BP1515 Lomé, Togo, France
[b] SYMME, Université de Savoie, BP 80439, 74944 Annecy le Vieux Cedex, France
[c] Institut Néel/CRETA/CNRS, 25 Avenue des Martyrs, BP166-38042 Grenoble Cedex, France

ARTICLE INFO

Article history:
Received 15 March 2008
Received in revised form 18 June 2008
Accepted 22 June 2008
Available online 10 July 2008

Keywords:
Ni–Cu alloy
Oxidation
Isoconversion
Arrhenius parameters
Model fitting

ABSTRACT

The kinetic parameters, namely the triplet activation energy E_A, model function $f(\alpha)$ or $g(\alpha)$ and pre-exponential factor A of the oxidation of Constantan tapes in 1 atm of oxygen have been determined from both isothermal and non-isothermal thermogravimetry. For isothermal experiments, with temperatures ranging from 650 °C to 900 °C, the results from direct conversion of the weight increase as a function of the time and curve fitting, are compared with the isoconversion method. For the non-isothermal experiments, with heating rates from 1 °C/min to 20 °C/min, comparison is made between the Friedman differential method and the integral methods of Kissinger, Ozawa and Li and Tang. All methods give apparent activation energies with relative standard deviations as low as 3%. The results converge to the identification of three stages in the oxidation behaviour. A parabolic law for reaction extents α below 15% with $E_A = 246 \pm 7$ kJ mol^{-1}, $\ln A = 14.3$, is followed by two linear stages with $E_A = 244 \pm 4$ kJ mol^{-1} and $\ln A = 15.3$ for $0.18 < \alpha < 0.35$ and $E_A = 228 \pm 15$ kJ mol^{-1}, $\ln A \approx 13$ for $\alpha > 45\%$, respectively.

1. Introduction

The transport of current in high-temperature superconductors is conditioned to the deposition of the superconducting phase on a bi-axially textured metallic substrate [1]. Nickel tapes are widely used but for AC applications, the ferromagnetism of this metal introduces hysteretic losses which is a major drawback. For this reason, Ni–Cu substrates with copper content from 50 at.% to 90 at.% have been produced [2,3]. In this copper composition range, Girard et al. [4] have shown the ability to perform an adequate bi-axial texture on industrial Constantan alloy. During the coating process at high temperature, oxidation of the substrate may occur thus modifying the surface relation between the tape and the superconductor. The knowledge of the oxidation kinetics and mechanism of the metallic tape is then of major importance to try to prevent such surface oxidation which is detrimental to the epitaxial growth of the superconductor. Recent studies on the oxidation of copper-rich NiCu alloys at high temperatures and various oxygen pressures [5–7] focussed on the formation and the description of the oxide scale and support an approximately parabolic oxidation behaviour. Brückner et al. [8] found that the oxidation of Constantan films in air and argon atmosphere (with about 3 ppm oxygen) starts at 300–350 °C forming, in the final state NiO, CuO or mixed oxide. The work of Bertrand [9] was also devoted to high temperature corrosion of Constantan alloys. It is reported that the oxidation kinetics follow a parabolic law with however three steps in the scale formation having different activation energies.

To investigate the oxidation mechanisms of Constantan tapes in 1 atm of oxygen, we conducted a kinetic analysis based on thermogravimetry. We followed as close as possible the procedures used in the ICTAC Kinetic Project for the study of the calcium-carbonate decomposition [10–14]. This paper presents the computational aspects of a study carried out to reach the characteristic triplet of the oxidation reaction: activation energy E_A, model function $f(\alpha)$ or $g(\alpha)$ of the reaction extent α and the pre-exponential factor A. It constitutes the first part of a general study on the mechanisms which govern the oxidation of Constantan tapes, with a comparison between the behaviour of as rolled and re-crystallized samples and a discussion on the role of impurities on the oxidation kinetics.

2. Theoretical considerations

The kinetics of solid-state reaction processes is usually governed either by nucleation and growth or by grain boundary reactions or by diffusion of the reacting species. The theoretical support for the kinetic analysis may be found in textbooks [15,16] and numerous recent reviews [17–22]. Let us summarize here the methods used in this work. By definition, the experimental part of the study of a reaction kinetics consists in determining the extent of the reaction α ($0 \leq \alpha \leq 1$) as a function of the time. This is described by the

* Corresponding author. Tel.: +33 450 096 518; fax: +33 450 096 543.
E-mail address: jean-louis.jorda@univ-savoie.fr (J.-L. Jorda).

0040-6031/$ – see front matter © 2008 Elsevier B.V. All rights reserved.
doi:10.1016/j.tca.2008.06.017

reaction rate ($d\alpha/dt$) which contains information on both the mechanism and the probability of occurrence of the reaction. Indeed, the reaction rate is generally expressed as a product of two functions:

$$\left(\frac{d\alpha}{dt}\right) = f(a)\cdot k(T) \quad (1)$$

- $f(\alpha)$ describes the analytic form of the limiting mechanism of the kinetic model; it is associated to the corresponding integral function $g(\alpha) = \int d\alpha/(f(\alpha))$. Different mathematical expressions account for the various mechanisms [23].
- $k(T)$, usually set as an Arrhenius-type function $k(T) = A\exp(-E_A/RT)$, is temperature-dependent and is related to the pre-exponential factor A and to the apparent activation energy E_A. R is the gas constant. Theoretical support for this assumption has been given by Galwey and Brown [24].

In the case of thermogravimetric measurements, $\alpha(t)$ is defined as $\alpha(t) = (m(t) - m_0)/(m_\infty - m_0)$ where $m(t)$, m_0 and m_∞ are the sample masses at time t, at the beginning of the experiment and when the reaction is completed, respectively. Our study concerns the oxidation behaviour of Ni–Cu–Mn alloys; m_∞ was calculated considering that metals are transformed into Cu(II), Ni(II) and Mn(II) oxides. This assumption may be discussed with the possibility to form the Cu(I) oxide but we shall see in the second part of this series of papers that it is largely supported by our optical and electronic metallographies as well as by XRD which show that Cu_2O represents less than 20% of the total amount of copper oxide after oxidation whatever the α-value. The error on α is then less than 0.5%.

Isothermal experiments have been considered for long time to be more accurate than non-isothermal heating but the increase in sensibility of the temperature and weight sensors allows the use of small samples in which heat exchange may be considered as instantaneous so that non-isothermal experiments are now widely used. Both processes may be associated with an isoconversional analysis of the data which gives access to E_A even if the reaction mechanism $f(\alpha)$ is not known. Eq. (1) may be written as

$$\ln\left(\frac{d\alpha}{dt}\right) = \ln[A\cdot f(\alpha)] - \frac{E_A}{RT} \quad (2)$$

For a given α-value, this quantity changes linearly with the inverse of temperature $1/T$ and E_A is readily deduced from the slope $-E_A/R$. For isothermal analysis the approach is straightforward. For non-isothermal experiments, the temperature increases as $T = T_a + \beta t$ with T_a, the ambient temperature and β the heating rate. The $\ln(d\alpha/dt)$ versus $1/T$ analysis for a given α and different β experiments is known as the Friedman method [25]. To calculate the integral form of the kinetic equation $g(\alpha) = \int k(T)\cdot dt$, it is usual to expand the Arrhenius function. We have used in this work two approximations known as the Kissinger [26] and the Ozawa [27] models and also the direct integral isoconversion method proposed by Li and Tang [28]. The underlying mathematics for these procedures are summarized in Table 1.

Table 1
Summary of relations used in this work for the isoconversional treatment of non-isothermal reaction kinetics

Method	Equation	Ref.
Friedman	$\ln\left(\frac{d\alpha}{dt}\right) = \ln[f(\alpha)\cdot A] - \frac{E_A}{RT}$	[25]
Kissinger	$\ln\left(\frac{\beta}{T_\alpha^2}\right) = \ln\left(\frac{AR}{E_A}\right) - \ln[g(\alpha)] - \frac{E_A}{RT_\alpha}$	[26]
Ozawa	$\ln\beta = \ln\frac{AE_A}{R} - \ln[g(\alpha)] - 2.315 - 1.0516\cdot\frac{E_A}{RT_\alpha}$	[27]
Li and Tang	$\int_0^\alpha \ln\left(\frac{d\alpha}{dt}\right) d\alpha = -\frac{E_A}{R}\int_0^\alpha \frac{d\alpha}{T} + G(\alpha)$	[28]

All these methods are efficient to compute E_A which is expected to be independent from the reaction extent α, in the case of a single reaction mechanism [29,30]. For a known E_A and a given $f(\alpha)$ or $g(\alpha)$ function, the pre-exponential factor A can be calculated from one of the expressions given in Table 1.

The experiments also give access to the reaction model by fitting $g(\alpha)$ on the basis of the known kinetic functions [24]. For isothermal analysis, the solution of the integral form of the kinetic equation is

$$g(\alpha) - g(\alpha_0) = \int_{t_0}^{t} k(T)\,dt = k(T)\cdot(t - t_0) \quad (3)$$

in which α_0 and t_0 are the extent of reaction and the time at the beginning of the temperature plateau, respectively. As already mentioned, $g(\alpha)$ reflects the limiting mechanism for instance species diffusion for which parabolic, linear and logarithmic laws have been found to satisfactory describe the oxidation kinetics of many metals and alloys at least in part of the reaction extent range.

To find $f(\alpha)$ and $g(\alpha)$ from non-isothermal experiments, it is necessary to use complementary model functions $y(\alpha)$ and $z(\alpha)$ introduced by Malek et al. [21] and derived from the $\alpha(t)$ data.

3. Experimental

The $Cu_{54}Ni_{45}Mn_1$ alloy (Constantan) was purchased from Goodfellow as 8-mm diameter cylinders. Besides copper and nickel, the manufacturer indicates 7500 ppm Mn and 2500 ppm Fe, present as impurities. Cold rolling was realised on a Redex rolling mill to a final thickness of 150 μm which corresponds to a deformation of 98.4%.

Fifty metal tapes were cut into 1 cm × 2 cm samples about 260 mg in weight. These samples were degreased in ethanol prior to oxidation. The thermogravimetric data were recorded at P_{O_2} = 1 bar using a SETARAM TG 92 apparatus. The samples were hung in the working zone of the apparatus with a platinum wire. For isothermal experiments, the sample temperature was rapidly (50 °C/min) raised to the desired plateau value between 650 °C and 900 °C and then kept constant for a maximum of 10 h. Because the temperature was raised in 1 bar O_2, the early stage of the oxidation – 0.1–2% in α depending on the plateau temperature – could not be analysed. For non-isothermal experiments, the temperature was raised to 900 °C with heating rates β between 1 °C/min and 20 °C/min. A gold tape used as blank was monitored for buoyancy corrections, found to be less than 0.3% in α. The results expressed in α terms are reported in Fig. 1 for isothermal from 650 °C to 900 °C (Fig. 1a) and non-isothermal (Fig. 1b) experiments.

4. Kinetic analysis

4.1. Isothermal process

4.1.1. The α(t) behaviour

The oxidation of Ni–Cu alloys has been claimed to imply diffusion through a Cu_2O/NiO scale [31]. A glance on the $\alpha(t)$ curve after an isothermal oxidation is a simple way to start the analysis. An example is given in Fig. 2 which represents the reaction extent $\alpha(t)$ as a function of the time at T = 875 °C.

It may be seen that parabolic oxidation is only acceptable in the domain (I) of the graph which corresponds to $\alpha < 15\%$. For higher α values, a linear behaviour is observed with a change of slope $k(T)$ at α = 35–45%, considered as a transition region.

4.1.2. Apparent activation energies

In the parabolic domain (region I in Fig. 2), the isothermal oxidations of tapes with a given surface area S are represented

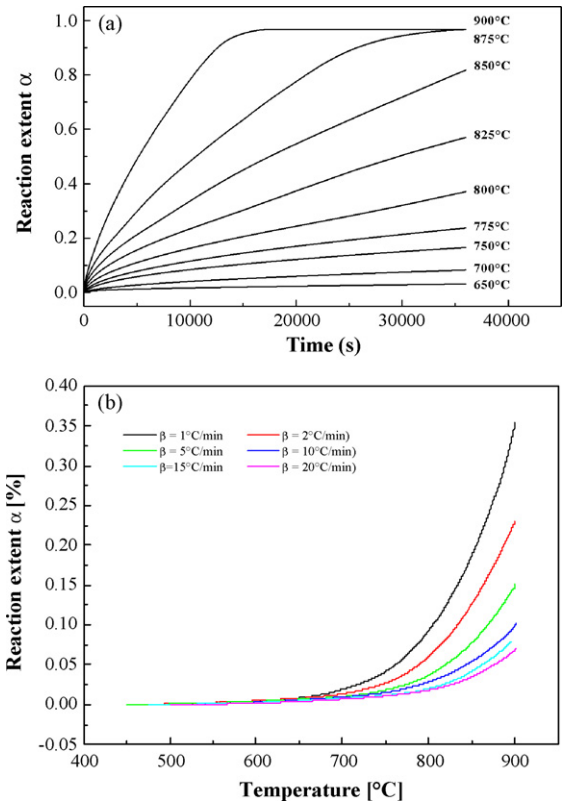

Fig. 1. Oxidation of Constantan in oxygen (P_{O_2} = 1 bar): (a) isothermal and (b) non-isothermal.

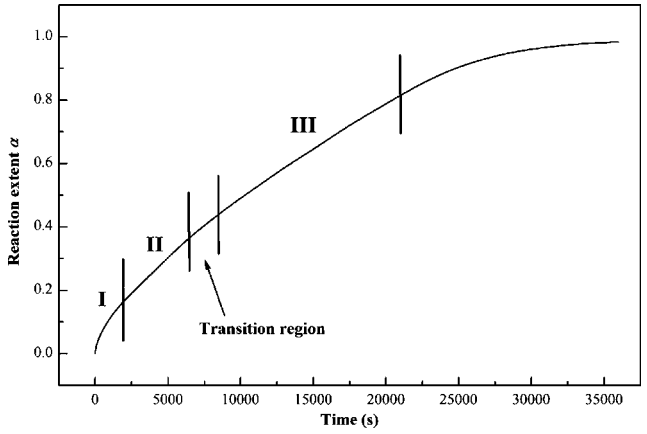

Fig. 2. Isothermal oxidation of Constantan at 875 °C.

in Fig. 3. The results are given as $(\Delta m/S)^2$ versus t from which the Arrhenius constant $k_p(T)$ may be computed (Table 2). In this table, the maximum α values for parabolic behaviour have been indicated.

Table 2
Arrhenius constant $k_p(T)$ for the isothermal oxidation of Constantan

Temperature (°C)	α Min %	α Max %	$k_p(T)$ (mg^2 cm^{-4} s^{-1})
650	0.56	4	8.2×10^{-6}
700	0.84	9	6.4×10^{-5}
750	1.07	18	2.4×10^{-4}
775	1.25	18	4.8×10^{-4}
800	1.52	19	1.0×10^{-3}
825	1.90	18	1.7×10^{-3}
850	2.43	20	2.9×10^{-3}

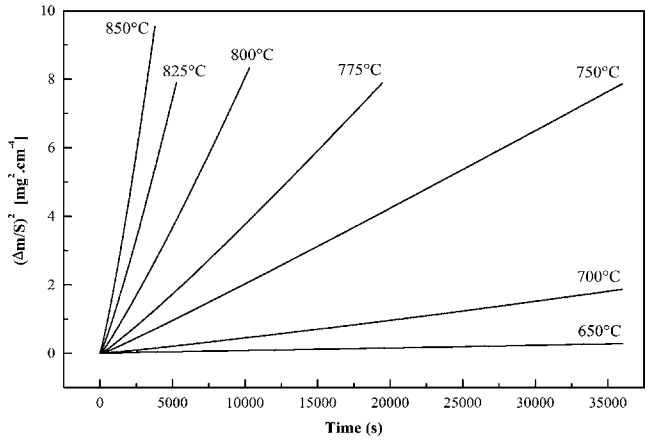

Fig. 3. Isothermal oxidation of Constantan in the parabolic regime.

From these results, the apparent activation energy E_A in the parabolic regime of the oxidation of Constantan is found to be $E_A = (251 \pm 5\ \text{kJ mol}^{-1})$.

The curves in Fig. 3 were obtained once the temperature plateau was reached, 12–18 min after the heating started. The corresponding minimum α values have been reported in Table 2. Since the parabolic oxidation of Constantan samples is not a general rule in the whole α-range, isoconversion analysis has been used to better define the limits for which a given model may be considered. As explained in Section 2, in such model-free method, the activation energy for each α-value is deduced from $\ln(d\alpha/dt)$ versus $1/T$ plots. The result is shown in Fig. 4.

We can clearly distinguish two main domains with different activation energies. The first one extends up to about $\alpha = 35\%$ with $E_A = (240 \pm 5\ \text{kJ mol}^{-1})$. It corresponds to the parabolic and the first linear regime of the oxidation. The second linear behaviour, above $\alpha = 35\%$, is characterized by a slightly but significantly lower activation energy $E_A = (220 \pm 5\ \text{kJ mol}^{-1})$.

4.1.3. Curve fitting: the kinetic model and the frequency factor

We now reconsider the isothermal $\alpha(t)$ change such as the one reported in Fig. 2, from which we have roughly delimited the different domains for the oxidation. The succession of regimes as time and reaction extent increase is even more evidenced with a log–log plot of $d\alpha/dt$ versus time (Fig. 5; $T = 850$ °C).

The parabolic regime is characterized by reaction rates $d\alpha/dt$ varying as $t^{-1/2}$. Of course, $d\alpha/dt$ remains constant in the case of

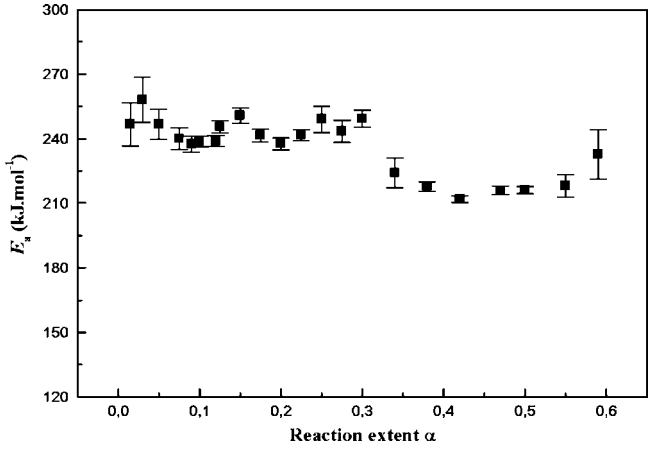

Fig. 4. Activation energies from the isoconversion analysis of isothermal data against the extent of reaction α.

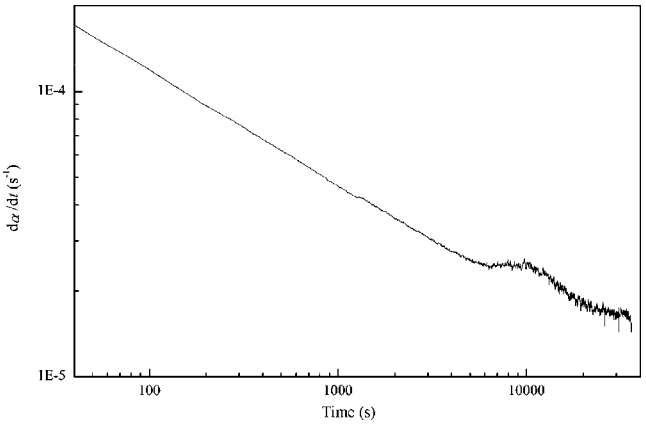

Fig. 5. Log–log plot of dα/dt vs. time at 850 °C showing the three different regimes: parabolic below 7000 s (α < 15%), linear between 7000 s and 12 000 s (15% < α < 35%) and linear with a lower $k(T)$ value above 20 000 s (α > 45%).

a linear regime. Below 7000 s (α < 15%), the curve shows a linear decrease of log(dα/dt) with log(t) with a slope close to −1/2. Then dα/dt remains constant, first between 7000 s and 12 000 s (15% < α < 35%) and also above 20 000 s (α > 45%) which denotes linear behaviours with however slightly different $k(T)$ values. It should be stressed for further analysis of the oxidation mechanism that the transition from the first linear regime to the second one is not abrupt but takes about 2 h at 850 °C, *i.e.* occurs in the 35–45% α-range. Moreover, for all investigated temperatures (650 °C < T < 900 °C), the transitions from one regime to the other were found to occur for the same α values so that we have:

- a parabolic oxidation below α = 15–18%,
- a first linear oxidation between α = 15–18% and 35%,
- a second linear oxidation above α = 45%,
- a very smooth transition between the two latter regimes.

For each temperature and each domain, curve fitting has been used to estimate $k(T)$ and then E_A and A from ln($k(T)$) versus 1/T plots (Fig. 6 and Table 3).

We have also summarized in Table 3 the values for the couple E_A–A obtained from isoconversion analysis. The consistency of the two mathematical treatments has to be noticed. Similarly it is worth pointing out the low values of the standard deviations generated by the calculations, excepted for the second linear domain in the curve fitting method, which is covered with only four temperatures (Fig. 6c)

Once the model functions $f(\alpha)$ and their validity range have been ascertained, the value of the pre-exponential factor can be deduced from isoconversion analysis for each reaction extent. The corresponding results are shown in Fig. 7 where the two main domains noticed in Fig. 4 for the apparent activation energies may be recognized.

Table 3
E_A and ln(A) values deduced from $\alpha(t)$ fits

Domain	Curve fitting method		Isoconversional method	
	E_A (kJ mol^{-1})	Ln(A)	E_A (kJ mol^{-1})	Ln(A)
Parabolic	242 ± 6	14.4 ± 0.6	244 ± 7	14.7 ± 0.9
Linear I	241 ± 4	15.2 ± 0.5	244 ± 4	15.3 ± 0.5
Linear II	230 ± 19	14 ± 2	220 ± 7	12.8 ± 0.7

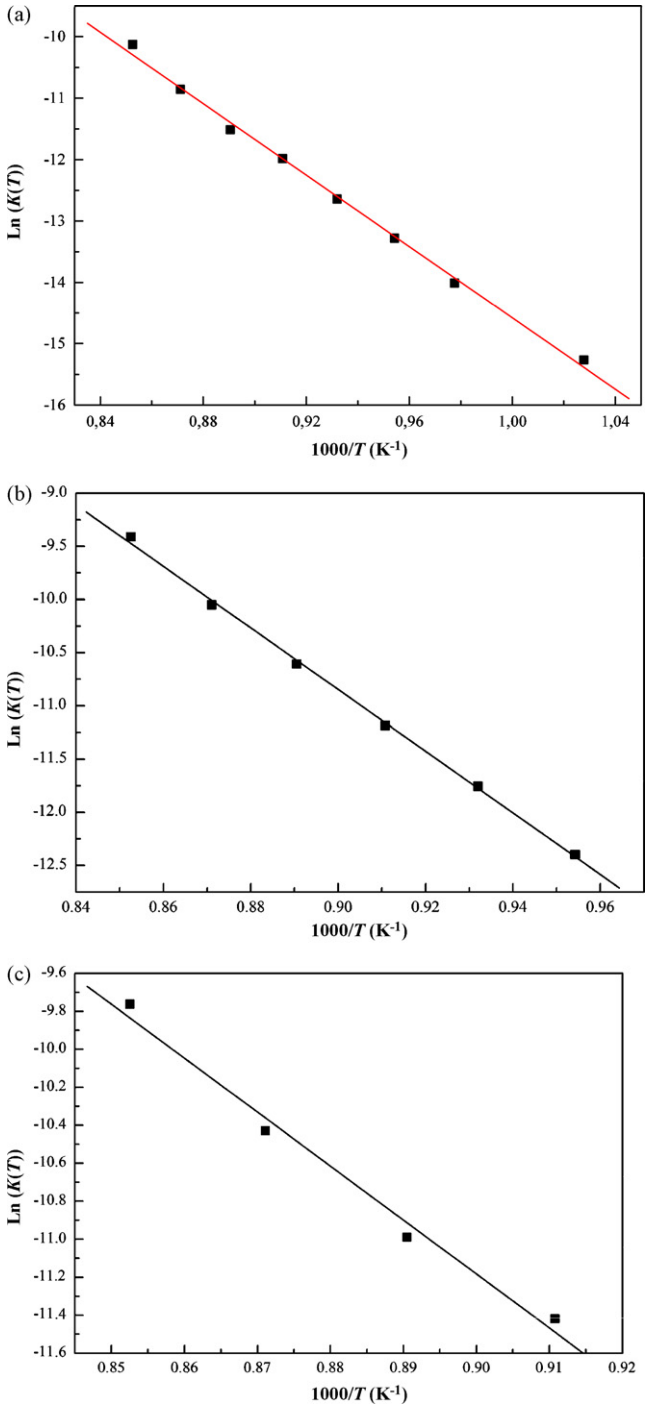

Fig. 6. Ln($k(T)$ against 1/T plots and linear fits for the calculation of E_A and ln(A) in the parabolic (a), first linear (b) and second linear (c) domains.

4.2. Non-isothermal methods

In non-isothermal methods the extent of the reaction depends on the heating rate β for a given final temperature. For the material studied here, coupled differential thermal analysis and thermogravimetry shown in Fig. 8 reveals that significant mass gain does not start below 450 °C. Complete oxidation of Constantan, when heated with β = 1 °C/min occurs at 1100 °C.

For lower temperatures, complete oxidation cannot be obtained (see Fig. 1b). In our experiments, the maximum α-value was about 40% for a heating rate β = 1 °C/min and a maximum temperature

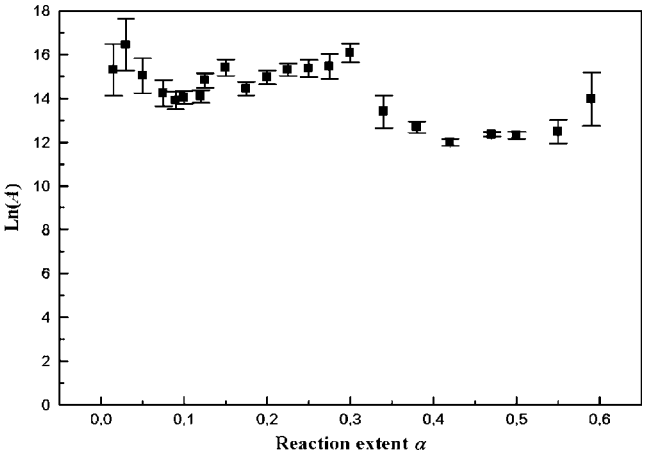

Fig. 7. Pre-exponential factor A as a function of reaction extent α as deduced from isoconversion for isothermal data.

of 900 °C. From the $\alpha(t)$ behaviour with various β, isoconversional analysis was performed. The results are displayed in Fig. 9 for the Friedman differential method [25] (Fig. 9a), the generalised Kissinger [26] (Fig. 9b) and the Ozawa [27] (Fig. 9c) integral methods for heating rates β from 1 °C/min to 20 °C/min and selected α-values from 0.5% to 12.5%.

Despite some scattering, the expected linear behaviour of the various functions versus $1/T$ is worth being pointed out. Using integral methods of Kissinger and Ozawa, the problem of the expansion of the temperature integral is raised and the "exact" value of this term is continuously under discussion [32]. For comparison, the Li and Tang method [28], free from integral approximation has been used. An example of $\ln(d\alpha/dt)$ and $1/T$ curves versus α with $\beta = 5$ °C/min is given in Fig. 10.

From such plots at various heating rates, numerical integration allows to represent $\ln t[\ln(d\alpha/dt) = \int_0^{\alpha} \ln(d\alpha/dt)\,d\alpha$ as a function of $\ln t[1/T] = \int_0^{\alpha}(1/T)\,d\alpha$. The results are straight lines with slope $-E_A/R$ shown in Fig. 11. Each group of points represents a reaction extent from 1% to 10% for linear heating rates ranging from 1 °C/min to 15 °C/min.

The activation energies for the oxidation of the Constantan tapes for each α value computed from all the above-mentioned non-isothermal methods are represented in Fig. 12. It may be seen that in the 1–15% range and within error limits, about 8 kJ mol^{-1} in each

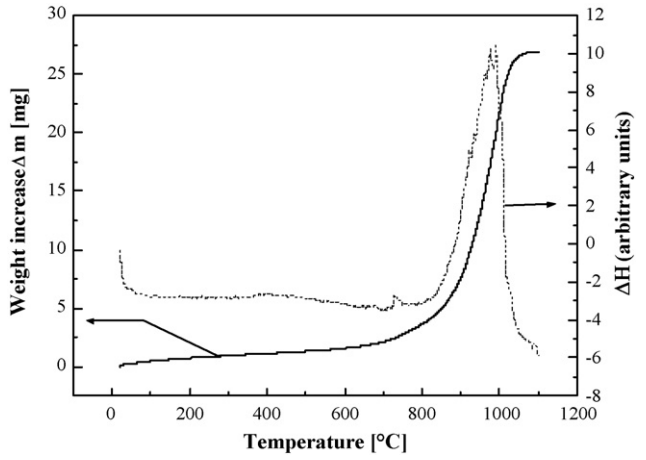

Fig. 8. Coupled differential thermal analysis (dashed curve)–thermogravimetry (bold) of the oxidation of Constantan in oxygen atmosphere with a heating rate $\beta = 1$ °C/min.

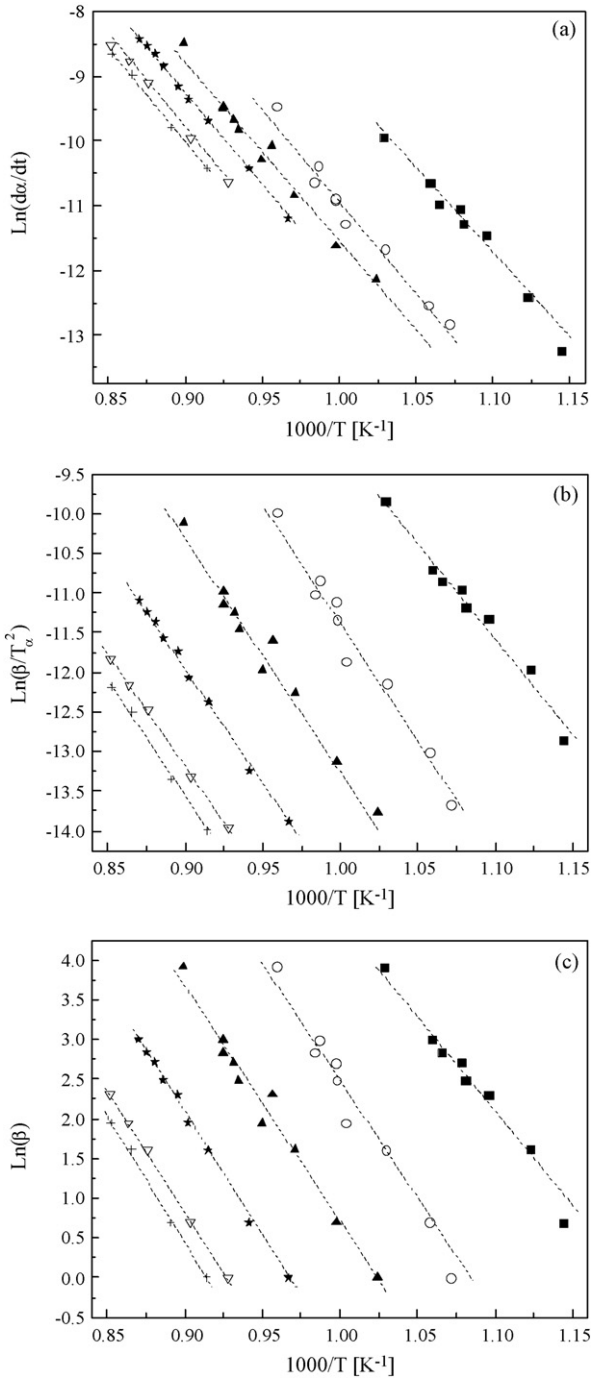

Fig. 9. Non-isothermal–isoconversion oxidation of Constantan. Differential Friedman method (a), integral Kissinger (b) and Ozawa (c) methods; $\alpha = 0.005$ (■); 0.01 (○); 0.02 (▲); 0.05 (⋆); 0.1 (▽) and 0.12 (+).

case, the apparent activation energy does not depend on the reaction extent. The mean value of all reported E_A is 243 kJ mol^{-1} with a standard deviation $\sigma = 15$ kJ mol^{-1}.

The agreement with the results obtained from isothermal experiments in the same α-range, as well as the accuracy for each method underline the coherence of the measurements and, moreover, suggest that oxidation proceeds with a single limiting mechanism.

In our isothermal studies we found that below $\alpha = 15\%$, the oxidation follows a parabolic law, suggesting a D1 diffusion mechanism for which the $f(\alpha)$ function is $f(\alpha) = 1/(2\alpha)$ and the integral function $g(\alpha) = \alpha^2$. In non-isothermal studies, it is possible to compute

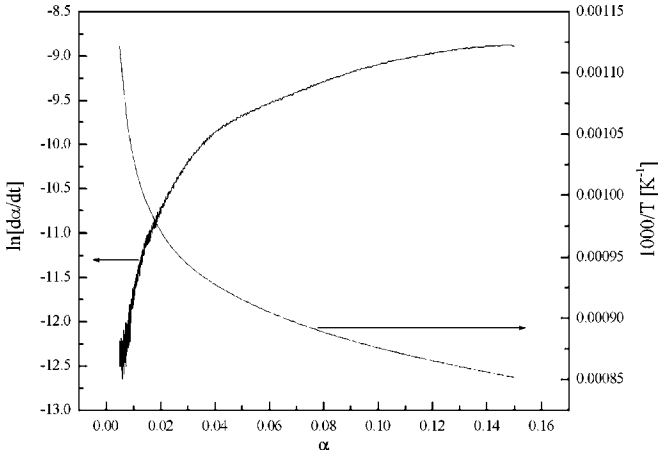

Fig. 10. Ln (dα/dt) and 1000/T as a function of α for a heating rate β = 5 °C/min used for the Li and Tang integral method.

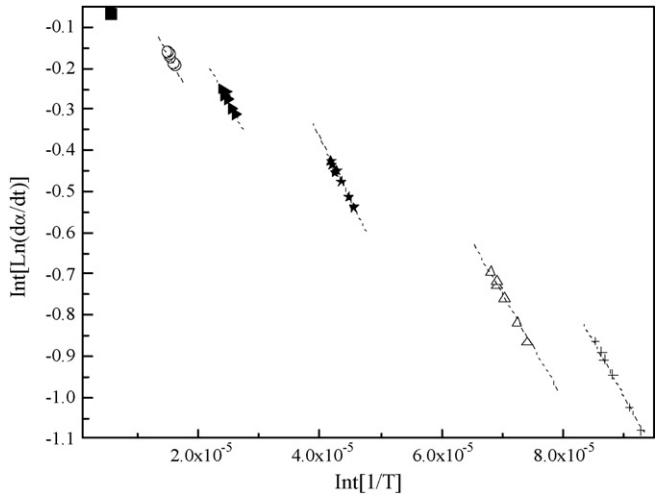

Fig. 11. Li and Tang analysis for the oxidation of Constantan; α = 0.01 (■); 0.02 (○); 0.03 (▲); 0.05 (★); 0.08 (▽) and 0.1 (+).

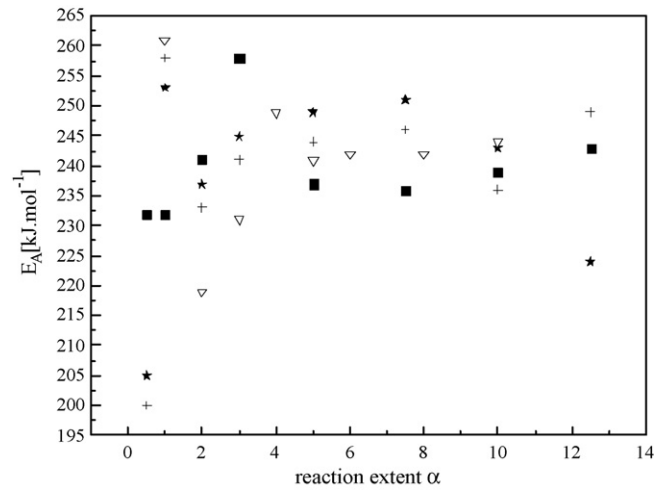

Fig. 12. Summary of the activation energies E_A from Friedman (■), Kissinger (+), Ozawa (★)and Li and Tang (▽) methods.

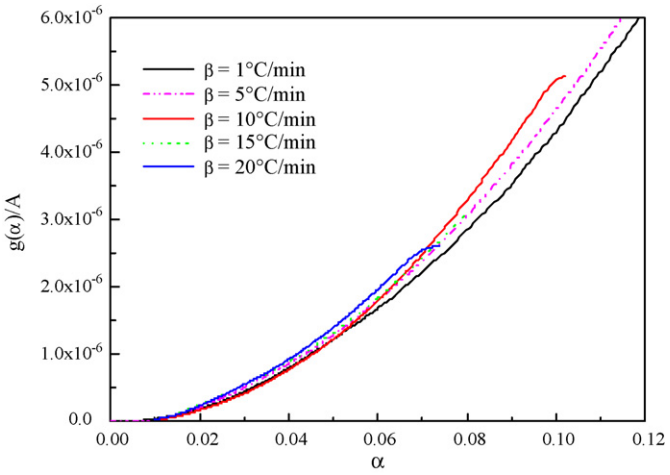

Fig. 13. Fitting of the non-isothermal oxidation curve by the Malek method [21]. For β ranging from 1 °C/min to 20 °C/min, $g(\alpha)$ is proportional to α^n with $n = 1.9 \pm 0.1$.

the ratio $z(\alpha)/(By(\alpha)) = g(\alpha)/A$, where $z(\alpha)$ and $y(\alpha)$ are the functions introduced by Malek et al. [21]. Fig. 13 shows this ratio as a function of α for heating rates β between 1 °C/min and 20 °C/min. All curves could be fitted as $g(\alpha)/A = a\alpha^n$ with $n = 1.9 \pm 0.1$ and R^2 values larger than 0.999, in excellent agreement with the isothermal experiments, extending the model function for D1 mechanism downwards α = 0.01.

If, as suggested by all results for $1\% < \alpha < 15\%$, this diffusion mechanism assumption is accepted, it is possible to calculate the pre-exponential factor A using the relations given in Table 1. In Fig. 14, the ln A values from all methods are reported as a function of α.

The mean value of ln A from this series of experiments is $\ln A = 13.5 \pm 1$. If we exclude the values computed at low α for some methods, in particular for the Li and Tang method, the result in the parabolic range is $\ln A = 14.3 \pm 0.8$, exactly the same value as that determined from isothermal experiments.

5. Discussion

For the first time, a complete set of the kinetic parameters for the oxidation of Constantan have been determined following a proce-

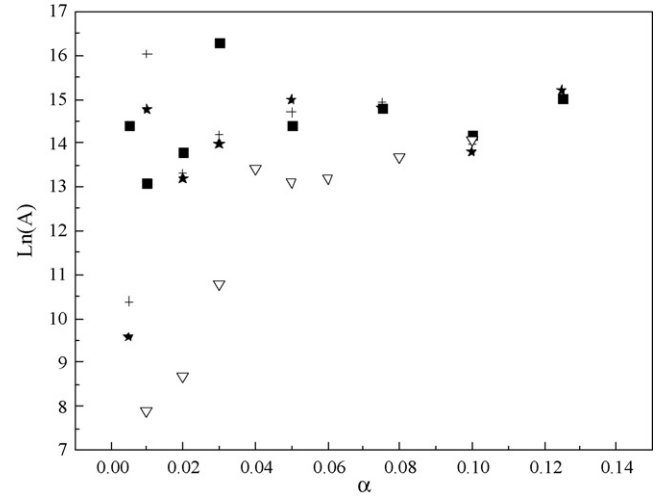

Fig. 14. The pre-exponential factor A obtained by Friedman (■), Kissinger (+) Ozawa (★) and Li (▽) methods.

Table 4
Summary of methods, models and Arrhenius kinetic parameters of the oxidation of Constantan

	α-Range	E_A (kJ mol^{-1})	Model $f(\alpha)$	Ln A
Isothermal process				
$\Delta m/S = [k(T)t]^n$	$\alpha < 0.18$	251 ± 5	$(2\alpha)^{-1}$	
Isoconversion	$0.02 < \alpha < 0.18$	244 ± 7	$(2\alpha)^{-1}$	14.7 ± 0.9
	$0.18 < \alpha < 0.35$	244 ± 4	1	15.3 ± 0.5
	$0.35 < \alpha$	220 ± 7	1	12.8 ± 0.7
Curve fitting	$0.02 < \alpha < 0.18$	242 ± 6	$(2\alpha)^{-1}$	14.4 ± 0.6
	$0.18 < \alpha < 0.35$	241 ± 4	1	15.2 ± 0.5
	$\alpha > 0.45$	230 ± 19	1	14 ± 2
Non isothermal process				
Isoconversion				
Friedmann	$\alpha < 0.20$	241 ± 7	$(2\alpha)^{-1}$	14.5 ± 0.9
Kissinger	$\alpha < 0.20$	244 ± 8	$(2\alpha)^{-1}$	14.6 ± 0.9
Ozawa	$\alpha < 0.20$	260 ± 7	$(2\alpha)^{-1}$	14.4 ± 0.7
Li and Tang	$\alpha < 0.20$	241 ± 12	$(2\alpha)^{-1}$	12 ± 2
Curve fitting (Malek) $g(\alpha)$		$g(\alpha) = C\alpha^n$ with $n = 1.9 \pm 0.1$		

dure described in the ICTAC kinetic project-data [10]. The samples for both isothermal and non-isothermal oxidation were taken from the same rolled batch. They were cut in similar dimensions and their weight did not differ by more than 3% from the mean value. For the computational step, the known kinetic models – see for instance Table 1 in [24] – have been tested in isoconversional or fitting methods. The coherence between the isothermal and non-isothermal Arrhenius parameters computed from 10 isothermal runs (between 650 °C and 900 °C) or 10 different heating rates (from 1 °C/min to 20 °C/min) give credibility to the results summarized in Table 4.

All the results converge to the following conclusions:

(i) The oxidation of the Constantan alloy is governed by a particle transport mechanism. However, a classical parabolic behaviour is not observed for the entire range of the reaction extent. It is restricted to $\alpha < 15$–18%. For higher α values, two successive linear laws are observed.
(ii) The Arrhenius parameters for each domain have been determined with a reasonable precision. A mean apparent activation energy $E_A = 246 \pm 7$ kJ mol^{-1} is found for the parabolic domain. A very close value is found using isothermal experiments for the first linear oxidation. For the second one, E_A is slightly decreased down to 228 kJ mol^{-1}. The distinction is not so clear for the frequency factor. Ln A ranges between 12 and 15.2 but in the parabolic field, both isothermal and non-isothermal experiments converge to ln $A = 14.3$ except for the Li and Tang method.
(iii) For non-isothermal experiments, we did not find any significant difference between the tested methods. All model-free differential or integral methods give similar Arrhenius parameters with similar accuracies. In addition, the different expansions of the temperature integral do not significantly affect the results.

These computational results have to be associated to mechanisms for the oxidation of copper–nickel alloys. This will be developed in a forthcoming paper but, for further discussion, it is necessary to keep in mind some results of the classical mechanism for the oxidation. Since the work of Wagner [33], it is accepted that the growth of an external oxide scale at the surface of metals and alloys follows a parabolic equation rate due to lattice diffusion. Hurlen [34] applied the absolute reaction rate theory to oxidation and derived a "general oxidation equation" in which the parabolic growth can be regarded as a limiting case amongst others, such as inverse logarithmic and cubic laws. In addition, for oxidation reactions, it is current to observe a linear kinetic law due to oxygen transfer through cracks in the oxide layer and voids in the oxide sublayer [35]. The change that we have observed between a parabolic and a linear law after the growth of the external oxide scale can be understood on this basis. More striking is the second change between the two linear regimes at about $\alpha = 35$–45%. It could be due crack closure after re-crystallization of the oxide grains.

The thermogravimetric study of the oxidation of bulk copper at high temperature under an oxygen pressure from 5×10^{-3} to 0.8 atm by Mrowec and Stoklosa [36] lead to an activation energy for oxidation of 200 kJ mol^{-1}. Kofstad [35] reports values ranging from 125 kJ mol^{-1} to 155 kJ mol^{-1}. For electro-deposited copper, Bertrand [9] determined $E_A = 126$ kJ mol^{-1}. For pure nickel the activation energies for the oxidation reported in the literature are lower, about 100 kJ mol^{-1} [9]. Recently, Haugsrud [37] distinguished a change in the oxidation kinetics of nickel depending on the temperature range, with $E_A = 150$ kJ mol^{-1} for $T < 800$ °C and $E_A = 200$ kJ mol^{-1} for $T > 1000$ °C. For Cu–10 wt.% Ni and Cu–15 wt.% Ni alloys, the oxidation at $T > 900$ °C is not perfectly parabolic [6] but the apparent activation energy is in the range 180–190 kJ mol^{-1}. For rolled commercial Constantan with a thickness of 50 μm, Bertrand [9] distinguished three successive steps in the oxidation: the formation of NiO, the formation of a copper oxide external layer and the internal oxidation by oxygen diffusion from the surface to the alloy with activation energies of 217 kJ mol^{-1}, 214 kJ mol^{-1} and 160 kJ mol^{-1}, respectively with standard deviations in the order of 16%. Qualitatively, our isothermal results are in agreement with these values. Moreover, the high accuracy of our results on the apparent activation energies ascertains the existence of three oxidation regimes and delimits the corresponding reaction extents. It is noteworthy that the apparent activation energies for the oxidation of Constantan are significantly higher than those reported for Cu–Ni alloys. The presence of Mn as impurity in Constantan has to be pointed out. To our knowledge no intermediate phase is reported in the Cu–Ni–Mn–O system but Cu(1+) and Mn(2+) have comparable ionic radii, 0.96 Å and 0.91 Å, respectively. The presence of Mn on some Cu sites in the Cu_2O phase formed in the oxide sublayer cannot be excluded, thus modifying the metallic vacancy distribution responsible of copper diffusion. This mechanism is thought to be the limiting mechanism in the first two steps for the oxidation of the alloy. Parabolic and linear behaviours only differ by the shortened

diffusion path when cracks are generated. In the last linear step of the oxidation, the change of the oxygen pressure inside internal pores may interfere with the copper diffusion, thus decreasing E_A by about 10%.

Concerning the frequency factor A, its evaluation depends both on the activation energy and the reacting mechanism defined by $f(\alpha)$ or $g(\alpha)$. The scattering of the $\ln A$ values is obviously related to the logarithmic and inverse temperature scales inherent to the Arrhenius fits. In addition, the dimension of A (s^{-1}) indicates that the pre-exponential factor has something to do with the reactivity [38,39], *i.e.* crystal-defects distribution and/or change of the reaction interface. Therefore, the possible change, during the oxidation of the sample morphology may affect A. However, the perfect agreement between the isothermal and non-isothermal values for $\ln A$ in the parabolic domain validates the results for the two subsequent linear domains. From the rate constants measured by Bertrand [9] for a similar alloy oxidised under $P_{O_2} = 1$ atm in the three regions she identified, we can calculate $\ln A = 17$, 17.3 and 12, respectively. The first two values are higher than ours, as expected, because of the lower values of the apparent activation energies she determined. The discrepancy could also be due to different sample thickness (50 μm for Ref. [9] compared to 160 μm in this study). For the third step of the oxidation, *i.e.* for $\alpha > 45\%$, $\ln A \approx 13$ seems to be a reasonable value (see Table 4).

For isoconversional analysis of non-isothermal experiments, our aim was also to compare the errors introduced in the evaluation of the kinetic parameters by the methods usually employed, differential or integral, and, in the last case, by the two approximations of the temperature integral $p(x) = \int_x^\infty ((\exp(-x))/x^2)\,dx$ where $x = E/RT$. Because of low oxidation kinetics, the comparison was only possible in the parabolic domain. Kissinger [26] approximated $p(x)$ as $p(x) = \exp(-x)/x^2$ and deduced an expression of $\ln(\beta/T^2)$ as a function of E/RT. Ozawa [27] used $p(x) = 0.0048\exp(-1.0516x)$ from which $\ln(\beta)$ is derived. Considering activation energies of about 200 kJ mol^{-1} and temperatures of the order 1000 K, *i.e.* $x \approx 20$, the two expansions differ by more than 30%. Some influence on the values of the kinetic parameters is then expected. In reality, Figs. 12 and 14 show that E_A and A calculated from the two methods are comparable. In addition, it is worth noting that the standard deviations over the results obtained from isoconversion are more dependent on the statistics (number of β values) than on the analytical model. In a critical review on the temperature integrals, Flynn [40] observed that the approximation used by Ozawa results in "large percentage deviations" from the correct value of E/RT. It is also the view of Starink [41] even if a correction algorithm has been developed by Opfermann and Kaisersberger [42]. In a more recent work, Gao et al. [32] discussed the errors introduced by the use of Kissinger and Ozawa approximations comparing with an "exact" temperature integral which in fact introduces a correction function to $p(x)$. Because we found similar results for all methods, we estimated that the use of such developments was not justified in this work. More questionable is the deviation observed at low α values for E_A and A. In fact, Figs. 12 and 14 show that for $\alpha < 0.02 - 0.03$, E_A and $\ln A$ for all integral methods are significantly lower than the mean values. It is particularly the case for the values obtained from the Li and Tang method. We guess that the discrepancy may be due to a phase diagram effect, a miscibility gap observed at $T < 354$ °C in the Cu–Ni system [43], or by stress relaxation of the laminated tapes influencing the initial stage of the oxidation. The Li and Tang method which uses a direct numerical integration of the experimental $\ln(d\alpha/dt) - \alpha$ and $(1/T) - \alpha$ curves may be more sensitive than analytical methods. The background noise observed in the curve $\ln(d\alpha/dt)$ versus α for $\alpha < 0.03$ in Fig. 10 supports this assumption.

6. Conclusion

The kinetic parameters for the oxidation of Constantan tapes have been determined from both isothermal and non-isothermal experiments using thermogravimetry. Direct mass measurements $(\Delta m/S)^2$, isoconversional and curve fitting methods have been applied to isothermal data for temperatures ranging from 650 °C to 900 °C. For non-isothermal studies, we used 10 different heating rates β for isoconversion analysis with one differential (Friedman) and three integral (Kissinger, Ozawa and Li and Tang) methods. All the measurements and calculations converge to the following results:

- The oxidation of Constantan tapes in 1 atm oxygen implies three different steps characterized by different evolutions of the reaction extent α with time. The first stage, up to $\alpha = 15$–18% is the well-accepted parabolic law which describes a 1D diffusion mechanism. The two subsequent stages ($\alpha = 18$–35% and $\alpha > 40$–45%) are both characterized by a linear increase of α with time with however different kinetic parameters.
- The activation energies have been determined with a relative standard deviation below 3%. In the parabolic and the first linear domains of $\alpha(t)$, the couple $E_A - \ln A$ is 246 kJ mol^{-1} – 14.7. Both values are slightly lower in the second linear regime.
- Both derivative and integral isoconversional methods applied to non-isothermal data provide the same results. When integral methods are used, the results for the activation energies are only slightly affected by the degree of expansion of the temperature integral.
- The characteristic regimes and the convergence of all mathematical treatments to the same kinetic parameters give credit to the existence of a specific limiting reaction mechanism for each domain. This first analytical stage is a prerequisite to the determination of the oxidation mechanism, which, on the basis of the physical and chemical characterizations of the samples, will be discussed in a forthcoming publication.
- From a methodological point of view, it is worth mentioning that both isothermal and non-isothermal techniques give very similar kinetic parameters when the recommendations and procedures suggested in the ICTAC project reports are respected.

Acknowledgement

The authors acknowledge financial support from the National Agency for Research (ANR) through the MADISUP program.

References

[1] A. Goyal, D.P. Norton, J.D. Budai, M. Paranthanan, E.D. Spech, D.M. Kroeger, D.K. Christen, Q. He, B. Saffian, F.A. List, D.F. Lee, P.M. Martin, C.E. Klabunde, E. Hartfield, V.K. Sikka, Appl. Phys. Lett. 69 (1996) 1795.
[2] A. Tussi, R. Corti, E. Villa, A.P. Bramley, M.E. Vickers, J.E. Evetts, Inst. Phys. Conf. Ser. 167 (2000) 399.
[3] B. de Boer, J. Eickemeyer, N. Reger, G-R.L. Fernandez, J. Richter, B. Hozapfel, L. Schultz, W. Prusseit, P. Berberich, Acta. Mater. 49 (2001) 1421.
[4] A. Girard, C.E. Bruzek, J.L. Jorda, L. Ortega, J.L. Soubeyroux, J. Phys. Conf. Ser. (EUCAS 2005) 43 (2006) 341.
[5] R. Haugsrud, P. Kofstad, Oxid. Met. 50 (1998) 189.
[6] R. Haugsrud, Corr. Sci. 42 (2000) 383.
[7] Y. Niu, F. Gesmundo, G. Farnè, Y.S. Li, P. Matteazzi, G. Randi, Corr. Sci. 42 (2000) 1763.
[8] W. Brückner, S. Baunack, G. Reiss, G. Leitner, Th. Knuth, Thin Solid Films 258 (1995) 252.
[9] C. Bertrand, PhD Thesis, University Reims-Champagne, Ardennes, 2000.
[10] M.E. Brown, M. Maciejewski, S. Vyazovkin, R. Nomen, J. Sempere, A. Burnham, J. Opfermann, R. Strey, H.L. Anderson, A. Kemmler, R. Keuleers, J. Janssens, H.O. Deysseyn, Chao-Rui Li, B. Tong, B. Tang, J. Roduit, T. Malek, Mitsuhashi, Thermochim. Acta 355 (2000) 125.
[11] M. Maciejewski, Thermochim. Acta 355 (2000) 145.
[12] S. Vyazovkin, Thermochim. Acta 355 (2000) 155.

[13] A.K. Burnham, Thermochim. Acta 355 (2000) 165.
[14] B. Roduit, Thermochim. Acta 355 (2000) 171.
[15] J. Sestack, Thermophysical Properties of Solids: Their measurements and Theoretical Analysis, Elsevier, Amsterdam, 1984.
[16] M.E. Brown, D. Dollimore, A.K. Galwey, Comprehensive Chemical Analysis, Elsevier, Amsterdam, 1980.
[17] E.J. Mittemeijer, J. Mater. Sci. 27 (1992) 3977.
[18] S. Vyazovkin, C.A. Wight, Ann. Rev. Phys. Chem. 48 (1997) 125.
[19] R. Serra, J. Sempere, R. Nomen, Thermochim. Acta 316 (1998) 37.
[20] S. Vyazovkin, C.A. Wight, Thermochim. Acta 340–341 (1999) 53.
[21] J. Malek, T. Mitsuhashi, J.M. Criado, J. Mater. Res. 16 (2001) 1862.
[22] B.V. L'vov, Thermochim. Acta 373 (2001) 97.
[23] A. Khawam, D.R. Flanagan, Thermochim. Acta 436 (2005) 101.
[24] A.K. Galwey, M.E. Brown, Proc. R. Soc. Lond. A 450 (1995) 501.
[25] H.L. Friedman, J. Polym. Sci. 66 (1965) 137.
[26] H.E. Kissinger, Anal. Chem. 29 (1957) 1702.
[27] T. Ozawa, Bull. Chem. Soc. Jpn. 38 (1965) 1881.
[28] C.R. Li, T.B. Tang, Thermochim. Acta 325 (1999) 43.
[29] J.D. Sevry, M.E. Brown, Thermochim. Acta 390 (2002) 217.
[30] J.R. Hopfermann, E. Kaisersberger, H.J. Flammersheim, Thermochim. Acta 391 (2002) 119.
[31] C. Wagner, J. Electrochem. Soc. 99 (1952) 369.
[32] Z. Gao, M. Nakada, I. Amasaki, Thermochim. Acta 369 (2001).
[33] C.Z. Wagner, Z. Physick. Chem. B21 (1933) 25.
[34] T. Hurlen, Acta Chem. Scand. 13 (1959) 695.
[35] P. Kofstad, High Temperature Corrosion, Elsevier Applied Science, 1988, p. 1.
[36] S. Mrowec, A. Stoklosa, Oxid. Met. 3 (1971) 291.
[37] R. Haugsrud, Corr. Sci. 45 (2003) 211.
[38] A.K. Galwey, M.E. Brown, Thermochim. Acta 300 (1997) 107.
[39] M.E. Brown, R.E. Brown, Thermochim. Acta 357–358 (2000) 133.
[40] J.H. Flynn, Thermochim. Acta 300 (1997) 83.
[41] M.J. Starink, Thermochim. Acta 404 (2003) 163.
[42] J. Opfermann, E. Kaisersberger, Thermochim. Acta 203 (1992) 167.
[43] D.J. Chakrabarti, D.E. Laughlin, S.W. Chen, Y.A. Chang, Binary Alloy Phase Diagrams, in: T.B. Massalski (Ed.) 2nd ed., ASM Int., 1996.